


Deformation-induced actuation of cells in asymmetric periodic flow fieldsSebastian W. Krauss , Pierre-Yves Gires , and Matthias Weiss **Experimental Physics I, University of Bayreuth, Universitätsstrasse 30, D-95447 Bayreuth, Germany*

(Received 4 October 2021; revised 4 June 2022; accepted 22 June 2022; published 8 August 2022)

Analyzing and sorting particles and/or biological cells in microfluidic devices is a topical problem in soft-matter and biomedical physics. An easy and rapid screening of the deformation of individual cells in constricted microfluidic channels allows, for example, the identification of sick or aberrant cells with altered mechanical properties, even in vast cell ensembles. The subsequently desired softness-specific segregation of cells is, however, still a major challenge. Moreover, aiming at an intrinsic and unsupervised approach raises a very general question: How can one achieve a softness-dependent net migration of particles in a microfluidic channel? Here, we show in a proof-of-principle experiment that this is possible by exploiting a deformation-induced actuation of soft cells in asymmetric periodic flow fields in which rigid beads show a vanishing net drift.

DOI: [10.1103/PhysRevFluids.7.L082201](https://doi.org/10.1103/PhysRevFluids.7.L082201)

The advent of microfluidic devices has fueled a multitude of experiments and applications, both in academia and industry [1–4]. In the biomedical context, high-throughput analyses of microfluidic droplets (“microreactors”) or individual cells have gained particular interest [3,5–7], not least as first steps towards future diagnostic usage. In this context, microfluidic devices for a rapid screening of individual cell stiffness [8,9] are supposedly among the most prominent applications with a great potential for analyzing blood and biopsy samples: Exposing cells in narrow channel segments to strong Poiseuille flows, the resulting deformations can be evaluated by rapid imaging of the cells’ contour lines as they pass the constriction one by one within a few milliseconds [8]. Using this approach, cells with aberrant mechanical properties, e.g., due to malignancy, sickle-cell disease, or malaria infections, can be detected even in complex cell mixtures such as whole-blood samples [10].

Going beyond mere screening, the key to further applications is a segregation of cells according to their mechanical properties. Using data from rapid imaging as an input for a downstream surface acoustic wave, cells have been shifted, for instance, into different arms of a y-shaped channel branching [11]. Yet, the need for high-speed (fluorescence) imaging with a sufficient quality, combined with an elaborate and sensitive feedback to address the acoustic wave, puts up the question whether a segregation and sorting of cells is also possible without any imaging by just exploiting the individual cell stiffness. This idea immediately raises a much more general and fundamental question: How can one achieve a softness-dependent net migration to differentiate particles with varying mechanical properties in a microfluidic channel?

Inspired by the principle of microscale ratchets that rely on spatially asymmetric periodic structures [12,13], it has recently been hypothesized that exploiting the deformation of soft particles in temporally asymmetric periodic Poiseuille flows can induce a softness-dependent net migration [14]: Driving particles in a microfluidic channel at a forward flow rate Q_1 for a time interval τ_1 , then (instantaneously) reverting the flow and reducing the flow rate to Q_2 for a time $\tau_2 > \tau_1$ leads to a

*Corresponding author: matthias.weiss@uni-bayreuth.de

restoration of the initial state of all fluid elements after a period $T = \tau_1 + \tau_2$ if $Q_1\tau_1 = Q_2\tau_2$. Since both the flow rate and the slip velocity of a rigid sphere are proportional to the flow curvature, any residual drift due to Faxen's law averages to zero over a period [15], i.e., nondeformable particles show no net drift after integer multiples of the period T . Soft particles, however, are deformed stronger during the first phase ($0 < t < \tau_1$) since $Q_1 > Q_2$, i.e., their effective extension perpendicular to the flow direction is reduced and hence they attain a higher effective drift velocity than rigid particles. In the restoration phase ($\tau_1 < t < T$) the deformation is less and the motion hence becomes more similar to rigid particles, eventually resulting in a net displacement Δx per period T . Formulating this qualitative argument more thoroughly, the existence of such a softness-induced actuation was indeed confirmed for idealized situations via analytical calculations and computer simulations [14]. Yet, an experimental verification that soft cells can indeed ratchet forward with each period, leaving stiff particles behind, has been lacking so far. Given that real-world applications are naturally plagued, for example, by finite relaxation times during flow reversal and complex material properties of individual cells, an experimental observation of the predicted segregation effect is in fact nontrivial.

Here, we close this gap and confirm the prediction of a deformation-induced actuation of soft particles in a proof-of-principle experiment. In particular, we have quantified the migration of rigid plastic beads and soft red blood cells (RBCs) in a microfluidic channel design with an optimized hydraulic resistance to facilitate a rapid relaxation upon switching/inverting flow rates (see Materials and Methods in the Supplemental Material [16] with additional references [17–21] for experimental details). As a result, we observed that beads did not show a significant net transport for integer multiples of the driving period T when applying symmetric or asymmetric periodic forward-backward flow profiles, whereas RBCs showed a marked actuation for an asymmetric driving. Our experiments therefore confirm the theoretically predicted possibility of a softness-induced segregation of particles. Based on our results, we discuss a future utilization of this effect in cell-sorting microfluidic devices.

As a first step of our experimental approach, we analyzed the shape of RBCs when subjecting them to different flow rates Q in a microfluidic channel (width $10\ \mu\text{m}$, height $100\ \mu\text{m}$). Representative bright-field images of RBCs at flow rates $Q = 800\ \mu\text{l/h}$ and $Q = 200\ \mu\text{l/h}$ are shown in Figs. 1(a) and 1(b). In line with previous observations [22,23], RBCs assumed a parachutelike shape that was enhanced at higher flow rates. Extracting the contour lines of RBCs [16] allowed us to determine their projected area A and perimeter ℓ , with which we quantified the overall deformation via the deviation of the circularity from unity,

$$\delta = 1 - \sqrt{\frac{4\pi A}{\ell^2}}. \quad (1)$$

This measure has also been used before for quantifying cell deformations in high-throughput experiments at very high flow velocities [8]. Confirming the visual impression, δ was significantly higher for $Q = 800\ \mu\text{l/h}$ than for $Q = 200\ \mu\text{l/h}$ [Fig. 2(c)]. Hence, switching flow rates induces different shapes of RBCs, as required as an ingredient for the described ratcheting process. As a next step, we probed whether rigid beads show a net drift over several cycles when imposing an asymmetrically oscillating forward-backward flow field. Here, we concentrated on a forward flow of $Q_1 = 1600\ \mu\text{l/h}$ for $\tau_1 = 10\ \text{s}$ and a backward flow of $Q_2 = 400\ \mu\text{l/h}$ for $\tau_2 = 40\ \text{s}$ [see Fig. 2(a)], yielding a period of $T = 50\ \text{s}$ after which the initial state should be restored. The microscope's field of view allowed for imaging 50–100 beads in every frame, situated at varying distances from the channel wall. Imaging and tracking these sets of beads at a frame rate of 140 Hz [16] allowed us to extract the beads' average velocity $\langle v(t) \rangle$ (averaged over the parabolic flow profile sampled by the beads' positions) as a function of time. Due to the finite number and length of tracks for each set of beads, the instantaneous average velocity showed some fluctuations, yet the temporal evolution of $\langle v(t) \rangle$ was clearly discernible [see Fig. 2(a) for a representative case]. As expected for a channel with finite hydraulic resistance, every flow reversal required a finite relaxation time

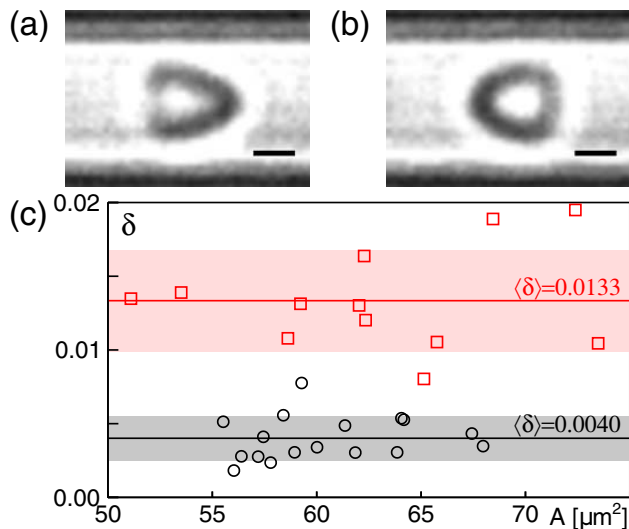


FIG. 1. Representative bright-field images of RBCs in a microfluidic channel (width $10 \mu\text{m}$, height $100 \mu\text{m}$) with flow rates (a) $Q_1 = 800 \mu\text{l/h}$ and (b) $Q_2 = 200 \mu\text{l/h}$ pointing to the right and left, respectively. Stronger deformations at higher flow rates are clearly visible; scale bar: $2 \mu\text{m}$. (c) Quantifying the cell deformation δ [Eq. (1)] confirms this visual impression: Deviations of individual RBCs from a circular shape (for which $\delta = 0$) were significantly larger for Q_1 (red squares) than for Q_2 (black circles). Solid lines and shaded regions indicate the respective mean and standard deviation.

for approaching the asymptotic velocity associated with the new flow rate. Consequently, $\langle v(t) \rangle$ needed a few seconds after each switching of the flow before reaching a plateau value. Therefore, even when minimizing the hydraulic resistance, the possibility to reduce τ_1 and τ_2 to small values remains limited (see also the discussion further below). Integrating $\langle v(t) \rangle$ over time yielded the oscillating average position $x(t)$ of the beads along the channel in response to the imposed flow field $Q(t)$. Results for an asymmetric and also a symmetric driving are shown in Fig. 2(b). In both cases, the minima in $x(t)$ did not show a progressive increase over several cycles, in contrast to what would be expected for an actuated motion. In accordance with this notion, quantifying the deviation from the initial position, after n periods, $\Delta x = x(nT) - x(0)$, did not show an increase for an increasing number of cycles [Fig. 2(c)] albeit a nonzero value was observed due to experimental imperfections.

Performing the same ensemble-based tracking approach for beads and RBCs in the same system resulted in a marked difference between these two entities (Fig. 3): The integrated averaged position $x(t)$ showed a clear shift of the minima positions for soft RBCs whereas stiff beads returned to their original position [see magnification in Fig. 3(a)]. Inspecting the associated profiles of the averaged velocity revealed that RBCs attained higher values for $\langle v(t) \rangle$ during the strong forward flow in the first phase ($nT < t < nT + \tau_1$). This discrepancy subsided for the softer backward flow during the second phase [$nT + \tau_1 < t < (n + 1)T$]. The resulting net shift of an ensemble of RBCs over several periods of the oscillating flow, quantified via the minima positions x_{\min} after integer multiples of T , was seen to grow linearly in time [Fig. 3(c)], in marked contrast to the restoring of bead positions [cf. Fig. 2(c)]. Thus, soft RBCs showed a significant net actuation in asymmetrically oscillating flows, as expected from theoretical considerations and despite the unavoidable imperfections in experiments. The segregation effect therefore can be deemed sufficiently robust to fuel applications.

So far, our evaluation approach relied on an ensemble average of many RBCs and beads. To complement these data, we also sought for a possibility to track individual RBCs, hence providing

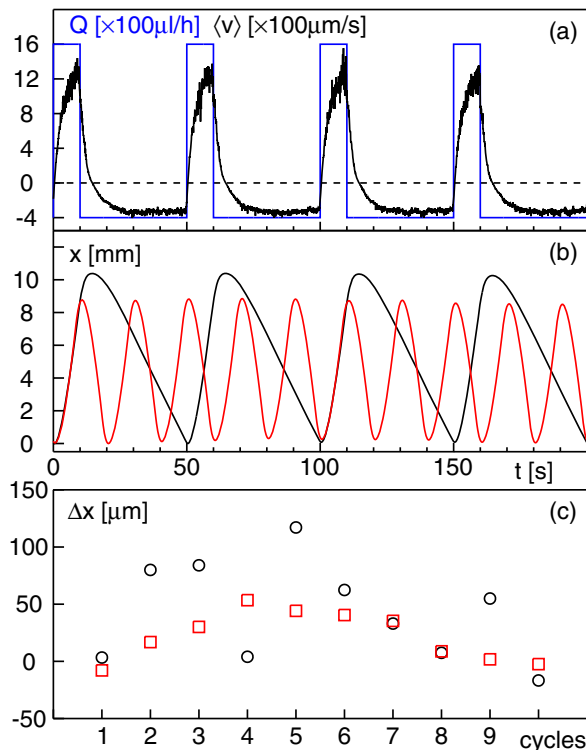


FIG. 2. (a) Applying a periodic and asymmetrically switching dichotomous flow rate $Q(t)$ in the microfluidic channel (blue line; forward: $Q_1 = 1600 \mu\text{l/h}$ for $\tau_1 = 10 \text{ s}$; backward: $Q_2 = 400 \mu\text{l/h}$ for $\tau_2 = 40 \text{ s}$) induces average maximum bead velocities that oscillate between plateau values $\langle v \rangle \approx +1.4 \text{ mm/s}$ and $\langle v \rangle \approx -0.4 \text{ mm/s}$ (black line). Please note that the periods τ_1 and τ_2 are sufficiently long to allow for a fair relaxation of the average velocity $\langle v(t) \rangle$ to the stationary value after reverting the flow. (b) Integrating $\langle v(t) \rangle$ over time yielded an average oscillatory excursion path $x(t)$ for this asymmetric periodic flow rate (black line). For comparison, the path obtained for a symmetrically switching flow rate ($Q_1 = Q_2 = 400 \mu\text{l/h}$ and $\tau_1 = \tau_2 = 10 \text{ s}$) is also shown (red line, multiplied by five for better visibility). In both cases, the minima in $x(t)$ do not show signatures of a net drift. (c) In line with this observation, the deviation $\Delta x = x(nT) - x(0)$ from the initial position after n cycles is nonzero in both cases due to experimental imperfections, but no progressive increase (as expected for an actuation) is observed. This is in qualitative and quantitative contrast to soft RBCs [cf. Fig. 3(c)].

access to the fluctuating actuation of individual cells. Since individual entities rapidly exit the microscope's field of view due to the imposed flow rates, a direct long-term tracking of all visited positions was not possible. We therefore used an alternative approach: When analyzing the acquired image series, we measured the time shift $\Delta T(n)$ that was needed in addition to the integer number of periods nT to position the very same individual RBC into its original locus in the field of view. Using the average velocity $\langle v(t) \rangle$ determined from the collection of beads to approximate the individual RBC's average velocity within one period [cf. Figs. 2(a) and 3(b)], this time shift was then translated into a traveled distance ξ that represents the net shift of this particular RBC along the channel after n periods. Accumulating the actuation over many periods can therefore be expected to yield a linear increase of the traveled distance, $\xi \sim \Delta T(n) \sim nT$. Inspecting the travel distance for individual RBCs (see Fig. 4 for representative examples) confirmed this very expectation. In favorable agreement with the aforementioned finding of an average net actuation of an RBC ensemble, also individual cells showed a displacement that grows linearly with the number

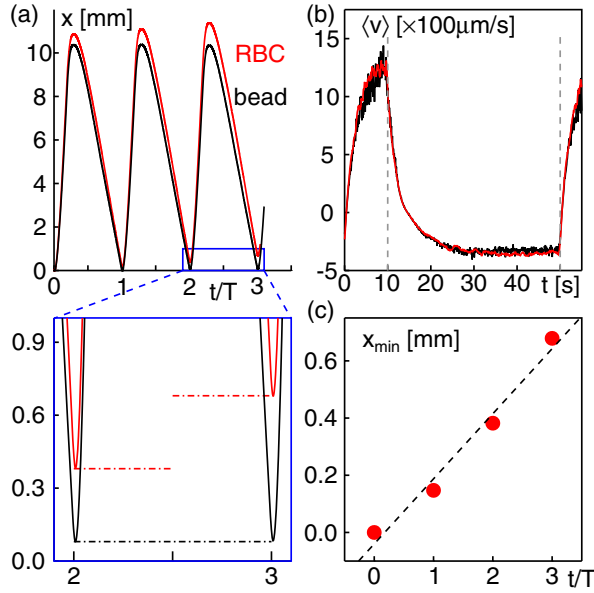


FIG. 3. (a) Comparing the ensemble-averaged position $x(t)$ of beads (black) and RBCs (red) in the same experiment reveals a marked progression of the minimum position for RBCs already after a few periods T (highlighted by the magnification in the blue rectangular region; dashed-dotted lines indicate the minima positions). (b) During the strong forward flow phase, RBCs attain a higher velocity than beads (red vs black line), whereas the softer but longer backward flow during the second phase is very similar. Gray dashed lines indicate the times at which flow rates were reverted. (c) As a result, RBCs show a significant net actuation from the initial position for progressing periods, as quantified via the minima positions $x_{\min}(nT)$ while beads remain basically at the initial position [cf. Fig. 2(c)]. The dashed line is a linear guide to the eye.

of cycles, but decorated with individual fluctuations that reflect the particular cell's size, stiffness, deformation profile, local tumbling, etc.

In summary, we have demonstrated here that subjecting soft RBCs to asymmetric oscillatory flow fields in a microfluidic channel can induce a net actuation that grows linearly with the number of driving periods, whereas stiff beads essentially show no net transport. This finding is in agreement

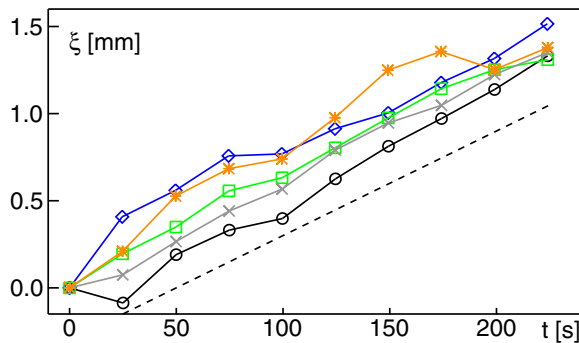


FIG. 4. Tracking individual RBCs (see main text and Supplemental Material [16] for details) reveals a net actuation ξ that grows linearly with the number of periods, in agreement with the average drift of an ensemble of RBCs displayed in Fig. 3(c). In addition, fluctuations around the linearly growing average reflect the individual cell's response to the deforming flow as RBCs vary in size, stiffness, etc.

with theoretical predictions for idealized systems [14] and provides a proof-of-principle case how such an unsupervised mechanism may be used to segregate particles according to their softness.

As a straightforward field of application, one may envisage using the effect in biomedical applications that require cell sorting according to stiffness. Here, the finite relaxation times after flow reversal, due to the hydraulic resistance, will certainly hamper a high-throughput scheme for individual cells, whereas a segregation of large cell ensembles within a reasonable time appears feasible. We have undertaken preliminary experiments along these lines, i.e., we aimed at separating a mixture of two populations of trypsinized HeLa culture cells, one of which was left untreated while the other had been subjected to pharmaceuticals (cytochalasin D and nocodazole) that disrupt all cytoskeletal structures and hence soften the cells. With our available experimental setup, we were unfortunately not able to segregate these two populations as the available flows were insufficient to significantly and differentially deform the cells, irrespective of the treatment. We attribute this somewhat disappointing observation to the cells' fairly rigid nuclei that occupy a large fraction of the volume and whose mechanical properties are hardly altered upon disrupting the cytoskeleton. Obtaining differential shape changes between the two cell populations therefore requires sufficiently strong shear stresses that deform the spherical shell of cytoplasm around the (unaltered) nuclei. While this had been achieved in previously described high-throughput devices with very strong Poiseuille flows [8,9], our setup and operation protocol with flow reversal did not allow us to reach this range. Future work will have to reveal, to which extent these technical limitations can be overcome for applications in the life sciences. Nevertheless, our experiments have demonstrated that soft capsules without a stiff internal nucleus (RBCs lack nuclei) can be deformed and sorted well, suggesting that a stiffness-dependent sorting of complex mixtures of simple soft capsules, used for example in the cosmetics industry, can be achieved with our inexpensive approach.

We thank W. Zimmermann and W. Schmidt for suggesting the experiments. Financial support by the VolkswagenStiftung (Az. 92738) and by the Elite Network of Bavaria (Study Program Biological Physics) is gratefully acknowledged.

-
- [1] G. M. Whitesides, The origins and the future of microfluidics, *Nature (London)* **442**, 368 (2006).
 - [2] E. K. Sackmann, A. L. Fulton, and D. J. Beebe, The present and future role of microfluidics in biomedical research, *Nature (London)* **507**, 181 (2014).
 - [3] M. Weiss, J. P. Frohnmayer, L. T. Benk, B. Haller, J. W. Janiesch, T. Heitkamp, M. Börsch, R. B. Lira, R. Dimova, R. Lipowsky, E. Bodenschatz, J. C. Baret, T. Vidakovic-Koch, K. Sundmacher, I. Platzman, and J. P. Spatz, Sequential bottom-up assembly of mechanically stabilized synthetic cells by microfluidics, *Nat. Mater.* **17**, 89 (2018).
 - [4] S. Neethirajan, I. Kobayashi, M. Nakajima, D. Wu, S. Nandagopal, and F. Lin, Microfluidics for food, agriculture and biosystems industries, *Lab Chip* **11**, 1574 (2011).
 - [5] A. B. Theberge, F. Courtois, Y. Schaerli, M. Fischlechner, C. Abell, F. Hollfelder, and W. T. S. Huck, Microdroplets in microfluidics: An evolving platform for discoveries in chemistry and biology, *Angew. Chem., Int. Ed.* **49**, 5846 (2010).
 - [6] R. Seemann, M. Brinkmann, T. Pfohl, and S. Herminghaus, Droplet based microfluidics, *Rep. Prog. Phys.* **75**, 016601 (2012).
 - [7] K. F. Sonnen and C. A. Merten, Microfluidics as an emerging precision tool in developmental biology, *Dev. Cell* **48**, 293 (2019).
 - [8] O. Otto, P. Rosendahl, A. Mietke, S. Golfier, C. Herold, D. Klaue, S. Girardo, S. Pagliara, A. Ekpenyong, A. Jacobi *et al.*, Real-time deformability cytometry: On-the-fly cell mechanical phenotyping, *Nat. Methods* **12**, 199 (2015).

- [9] P. Rosendahl, K. Plak, A. Jacobi, M. Kraeter, N. Toepfner, O. Otto, C. Herold, M. Winzi, M. Herbig, Y. Ge, S. Girardo, K. Wagner, B. Baum, and J. Guck, Real-time fluorescence and deformability cytometry, *Nat. Methods* **15**, 355 (2018).
- [10] M. Urbanska, P. Rosendahl, M. Kräter, and J. Guck, High-throughput single-cell mechanical phenotyping with real-time deformability cytometry, *Methods Cell Biol.* **147**, 175 (2018).
- [11] A. A. Nawaz, M. Urbanska, M. Herbig, M. Nötzel, M. Kräter, P. Rosendahl, C. Herold, N. Toepfner, M. Kubankova, R. Goswami, S. Abuhattum, F. Reichel, P. Müller, A. Taubenberger, S. Girardo, A. Jacobi, and J. Guck, Intelligent image-based deformation-assisted cell sorting with molecular specificity, *Nat. Methods* **17**, 595 (2020).
- [12] F. Jülicher, A. Ajdari, and J. Prost, Modeling molecular motors, *Rev. Mod. Phys.* **69**, 1269 (1997).
- [13] Q. Guo, S. M. McFaul, and H. Ma, Deterministic microfluidic ratchet based on the deformation of individual cells, *Phys. Rev. E* **83**, 051910 (2011).
- [14] W. Schmidt, A. Förtsch, M. Laumann, and W. Zimmermann, Oscillating non-progressing flows induce directed cell motion, *Phys. Rev. Fluids* **7**, L032201 (2022).
- [15] J. Happel and H. Brenner, *Low Reynolds Number Hydrodynamics: With Special Applications to Particulate Media*, Vol. 1 (Springer, Berlin, 2012)
- [16] See Supplemental Material at <http://link.aps.org/supplemental/10.1103/PhysRevFluids.7.L082201> for supplementary text on materials and methods with additional figures.
- [17] D. Flormann, O. Aouane, L. Kaestner, C. Ruloff, C. Misbah, T. Podgorski, and C. Wagner, The buckling instability of aggregating red blood cells, *Sci. Rep.* **7**, 7928 (2017).
- [18] T. M. Fischer, A method to prepare isotonic dextran-salt solutions, *Cytometry, Part A* **77A**, 805 (2010).
- [19] F. Carrasco, E. Chornet, R. P. Overend, and J. Costa, A generalized correlation for the viscosity of dextrans in aqueous solutions as a function of temperature, concentration, and molecular weight at low shear rates, *J. Appl. Polym. Sci.* **37**, 2087 (1989).
- [20] J.-Y. Tinevez, N. Perry, J. Schindelin, G. M. Hoopes, G. D. Reynolds, E. Laplantine, S. Y. Bednarek, S. L. Shorte, and K. W. Eliceiri, Trackmate: An open and extensible platform for single-particle tracking, *Methods* **115**, 80 (2017).
- [21] T. F. Chan and L. A. Vese, Active contours without edges, *IEEE Trans. Image Process.* **10**, 266 (2001).
- [22] R. Skalak and P. I. Branemark, Deformation of red blood cells in capillaries, *Science* **164**, 717 (1969).
- [23] H. Noguchi and G. Gompper, Shape transitions of fluid vesicles and red blood cells in capillary flows, *Proc. Natl. Acad. Sci. USA* **102**, 14159 (2005).